Appl Phys B (2011) 105:379–384
DOI 10.1007/s00340-011-4520-5

Applied Physics B
Lasers and Optics

Fabrication of hollow optical waveguides in fused silica by three-dimensional femtosecond laser micromachining

F. He · J. Lin · Y. Cheng

Received: 7 January 2011 / Revised version: 25 February 2011 / Published online: 7 May 2011

Abstract We report on the fabrication of hollow optical waveguides in fused silica using femtosecond laser micromachining. We show that in such hollow waveguides, high-intensity femtosecond laser beams can be guided with low optical loss. Our technique, which was established earlier for fabrication of optofluidic structures in glass, can ensure a high smoothness at the inner surfaces of the hollow waveguides and provide the unique capability of fabrication of hollow waveguides with complex geometries and configurations. A transmission of ∼90% at 633 nm wavelength is obtained for a 62-mm-long hollow waveguide with an inner diameter of ∼250 μm. In addition, nonlinear propagation of femtosecond laser pulses in the hollow waveguide is demonstrated, showing that the spectral bandwidth of the femtosecond pulses can be broadened from ∼27.2 to ∼55.7 nm.

1 Introduction

Hollow optical waveguides have become one of the key elements in high-field laser physics experiments, including pulse compression [1–3], high-order harmonic generation [4, 5] and laser particle acceleration [6, 7], etc. With the hollow waveguides, the confinement of high intensity optical beams can be maintained over a distance significantly longer than the Rayleigh length, thereby boosting the efficiency of nonlinear interaction in gas media through the extension of interaction length and/or improved phase matching condition. Currently, hollow waveguides are frequently fabricated by glass drawing technique which is inherently a one-dimensional (1D) technique. In some cases, hollow waveguides or capillaries fabricated by stacking two open microgrooves separately formed on the surfaces of substrates by femtosecond laser ablation are also used; however, usually the cross-sectional shapes of such capillaries are difficult to be precisely controlled and the roughness of the laser ablated inner surface is relatively high [8]. Here, we show that the above-mentioned issues can be overcome by fabrication of hollow waveguides using three-dimensional (3D) femtosecond laser microfabrication.

Fabrication of hollow structures buried in glass materials by femtosecond laser is a direct writing technique [9–11]. The fabrication process essentially consists of two key steps: (1) spatial-selective modification of the etching property of glass by scanning a tightly focused femtosecond laser beam inside glass; and (2) preferential removal of the material in the laser modified regions by chemical etching for creating the hollow structures. For fabrication of hollow structures in photosensitive glass Foturan [10, 11], post-annealing is necessary after the femtosecond laser direct writing in order to form an etchable phase in the femtosecond laser irradiated areas. However, the chemically etched inner surfaces always show a relatively high roughness; e.g., the average roughness is around ∼40 nm, which is still insufficient for most optical applications [12]. Therefore, an additional post-annealing technique is applied to the etched samples for further smoothening the inner surface [12, 13]. A similar technique for obtaining smooth surface fabricated by femtosecond laser micromachining is to polish the surface with an oxyhydrogen flame [14, 15]. However, the oxyhy-

F. He · J. Lin · Y. Cheng (✉)
State Key Laboratory of High Field Laser Physics, Shanghai Institute of Optics and Fine Mechanics, Chinese Academy of Sciences, P.O. Box 800-211, Shanghai 201800, China
e-mail: ycheng-45277@hotmail.com

J. Lin
Graduate School of the Chinese Academy of Sciences, Beijing 100039, China

drogen flame polish technique can only be used for open structures with their surface exposed. Therefore, for fabrication of buried hollow structures, post-annealing in an oven at a predetermined temperature is currently the only solution to achieve the sufficient inner-surface smoothness for optical applications.

2 Hollow waveguides fabrication

In our experiment, commercially available fused silica glass substrates (UV grade fused silica JGS1) with a size of 5 mm × 100 mm × 2 mm are used. To facilitate the observation of the fabricated structures embedded in the glass substrates, both the upper and bottom surfaces of samples are polished. Fabrication of the hollow waveguides includes three steps: (1) inscription of the waveguide inside fused silica chips with temporally focused femtosecond laser beam [16]; (2) etching of the samples in a solution of 20 M/L KOH diluted with water in ultrasonic bath for selective removal of the material in the modified areas [17]; (3) baking of the sample in a programmable furnace for smoothening of the surface. In the process of laser irradiation, the laser system consists of a Ti:sapphire oscillator (Legend, Coherent, Inc., USA) and a regenerative amplifier, which emits 800 nm, 40 fs pulses with maximum pulse energy of ∼2.5 mJ at a 1-kHz repetition frequency. For achieving a circular cross section for the hollow waveguide, a spatiotemporal focusing method is used. It should be noted that although the circular cross section can also be achieved with a slit-beam shaping or an astigmatic beam shaping technique in femtosecond laser direct writing [18, 19], these techniques require that the scan direction of the femtosecond laser beam must be parallel to the slit or the cylindrical lenses placed before the objective lens. In such case, fabrication of curved waveguides will be difficult. However, with the temporal focusing technique, we can fabricate not only straight optical waveguides but also curved waveguides with arbitrary geometries (e.g., the wavy waveguides as shown in Fig. 4). It should be noted that in order to create the spatiotemporally focused beam, a grating pair ruled with 1500 lines/mm and blazed at the wavelength of 800 nm is used to separate different spectral components, which is different from our previous work [16]. A 20× objective with a numerical aperture (NA) of 0.46 is used to focus the beam to a ∼2 μm spot. The average femtosecond laser power measured before the objective is ∼20 mW. These laser exposure conditions are chosen to ensure that the femtosecond laser fluence is about twice the dielectric breakdown threshold, and the adjacent pulses sufficiently overlap so that a high chemical etching rate can be obtained. More details of the experiment setup with spatiotemporally focused femtosecond laser beams can be found elsewhere [16].

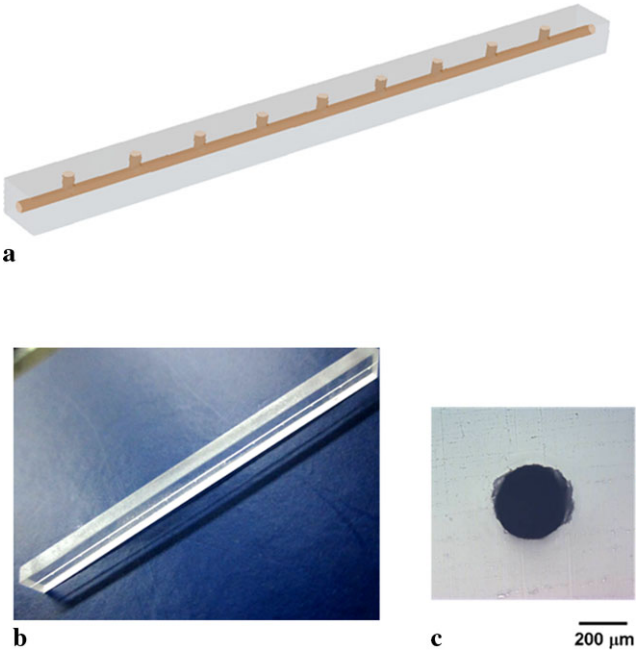

Fig. 1 (Color online) (**a**) Schematic of the hollow waveguide; (**b**) overview image of a 62-mm-long hollow waveguide captured by digital camera; (**c**) optical micrograph of the cross section of the hollow waveguide

The waveguide pattern is inscribed ∼500 μm beneath the surface, and the total length is 100 mm. For achieving a higher etching ratio, the waveguide is scanned three times with a speed of 100 μm/s. Since the contrast ratio of etching selectivity for a KOH solution between the laser exposed and unexposed regions is typically limited to 100–200 [17], we fabricate 21 short vertical channels with an equal interval of 5 mm between each other along the waveguide, as illustrated by the schematic in Fig. 1(a). The reason for fabricating the 21 vertical outlets is to ensure a homogeneous diameter of the hollow channel by reducing the taper caused by the limited selectivity of the etch ratio [10, 11]. On the other hand, increasing the number of vertical outlets along the channels will give rise to stronger light scattering for guiding the optical beam. We have tried different lengths for optimization of the interval between two adjacent outlets and found that ∼5 mm is the maximum interval for maintaining a nearly uniform diameter (e.g., small taper) of the channels.

After femtosecond laser irradiation, the sample is subjected to wet chemical etching in a solution of 20 M/L KOH diluted with water in an ultrasonic bath. The temperature of solution is kept to be 95°C constantly during the etching process. The hollow channel is formed after ∼20 h, while its average diameter is merely ∼30 μm. To achieve a hollow channel with a diameter of ∼250 μm, which is a typical size of the hollow fiber used for many high-field physics applications, the sample is further etched

for another ∼150 h. Since some reaction product may contaminate the channel during the etching process, the etched sample is ultrasonically cleaned in distilled water for ∼15 min. At this time, the roughness of the inner surface is very poor, which is unfavorable for optical applications.

To improve the surface smoothness of the sidewall of channel, we post-anneal the sample in a box-type furnace (HMF 1700-20, Shanghai, China). The furnace can provide an annealing temperature as high as 1700°C. It should be noted that although previously we have successfully reduced the inner-surface roughness of microstructures fabricated in Foturan glass using 3D femtosecond laser micromachining, smoothening of the inner surface of fused silica using a similar annealing method is achieved in this work for the first time to our best knowledge. The post-annealing protocol for smoothening the inner surface of fused silica is as follows: first, the temperature is ramped to 600°C at 5°C/min and then held at this temperature for 1 h; then the temperature is ramped from 600°C to 1200°C at 5°C/min and held at 1200°C for 5 h; finally the sample is cooled down to the room temperature at 5°C/min. The optimum annealing temperature of 1200°C is determined as a result of a trail and error process. Specifically, the intermediate step at 600°C is used for protecting the furnace according to the user's guide of the furnace, which may not be necessary for other types of furnaces. Figures 1(b) and 1(c), shows an overview image captured by digital camera and an optical micrograph of the cross section of the channel, respectively. The circular cross section should be attributed to spatiotemporal control of ultra short pulses during the laser irradiation process [16].

To quantitatively investigate the roughness improvement, we fabricate two hollow microstructures with a rectangular cross section under the same experimental conditions. For facilitating the scanning–probe microscopy examination, the rectangular-cross-section hollow structures are the structures without roof and floor, which are fabricated by scanning a femtosecond laser beam focused by a 20× objective lens (NA 0.46) layer by layer from the top to the bottom of the glass substrate. One of the samples undergoes the above-mentioned post-annealing for inner-surface smoothening, while the other does not. We then break the samples to have the laser-fabricated inner surfaces exposed, so that the surface roughness can be measured with optical microscopy and scanning–probe microscope (SPM). Even from the optical micrographs of the surfaces of these two samples (Figs. 2(a) and 2(b)), a dramatic improvement of inner-surface roughness can be observed. Moreover, scanning–probe micrographs of the inner surfaces fabricated without the post-annealing process are presented in Fig. 2(c) for a small area of 10 × 10 μm^2 and in Fig. 2(e) for a large area of 50 × 50 μm^2, and rough surfaces are

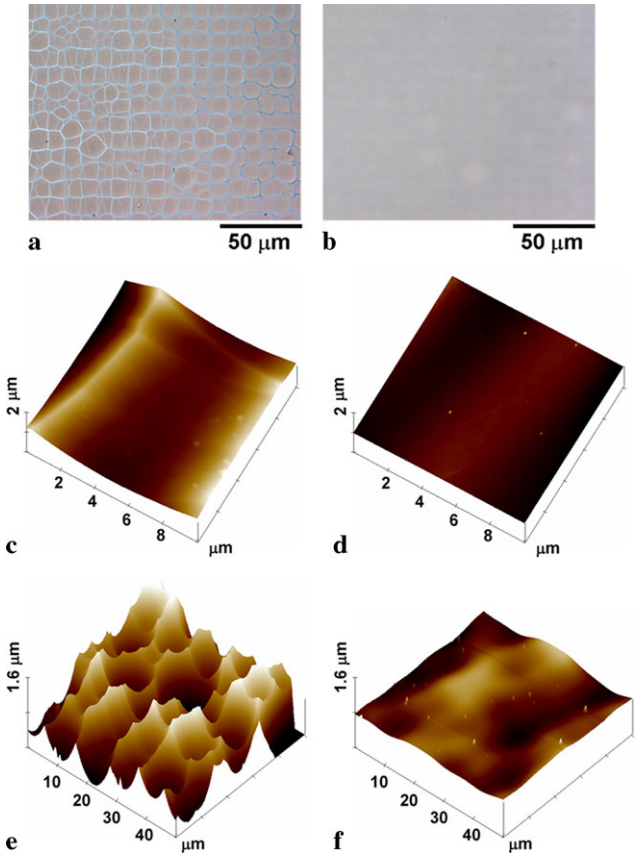

Fig. 2 (Color online) Optical micrographs of inner surfaces (**a**) before and (**b**) after annealing. SPM images of inner surfaces (**c**) before and (**d**) post-annealing for a small area of 10 × 10 μm^2; SPM images of inner surfaces (**e**) before and (**f**) post-annealing for a large area of 50 × 50 μm^2. The data of surface roughness are given in Tables 1 and 2

observed. For comparison, scanning-probe micrographs of the inner surfaces fabricated with the post-annealing process are presented in Figs. 2(d) and 2(f), for both the small and large areas mentioned above, respectively. Clearly, the surface smoothness is significantly improved by the post-annealing process. Quantitatively, as one can see from Tables 1 and 2, the average roughness (R_a) of the inner surface is greatly reduced from 101.5 to 4.6 nm by the annealing process for the small-area case, and from 277.5 to 44 nm by the annealing process for the large-area case. Particularly, it is noteworthy that the annealed surface in Fig. 2(e) exhibits a ripple structure with a regular period of a few microns which is responsible for the increased surface roughness measured with the large examination area. The reason of formation of such ripples remains unclear and deserves further investigation. The smoothened inner surface is critical for the optical waveguide applications.

3 Characterization of optical property of hollow waveguides

Before characterizing the optical properties of the waveguide, we first polish both ends of the sample and obtain a 62-mm-long hollow waveguide. We then inject a He–Ne laser beam at a wavelength of 632.8 nm into the waveguide. In this study, an optical lens with the focal length of 400 mm is used to achieve an optimal coupling. The diameter of the laser beam at the front surface of the lens is measured to be ∼4 mm. The input of the waveguide is placed 490 mm far from the lens. And the laser power measured after the lens (but before the waveguide) is ∼18.53 μW, while the output power measured after the waveguide is 16.56 μW. Thus the total transmission of the waveguide reaches ∼89.4%, whereas the maximum transmission calculated using (33)–(34) in Ref. [20] is ∼95%. We attribute the discrepancy between the experimentally measured and the calculated losses to the following two factors: (1) the light scattering at the sidewall of the fabricated hollow waveguide, and (2) the extra coupling loss caused by the deviation of the focused incident beam from the ideal Gaussian beam (the ideal Gaussian beam is used for evaluating the coupling loss). We also capture the images of both the near-field and far-field modes of the waveguide using a CCD camera, as shown in Fig. 3. One can clearly see that the output beam has a single-mode profile.

As we have mentioned in the Introduction, fabrication of hollow optical waveguides by femtosecond laser micromachining is flexible and in principle allows for fabrication of hollow waveguides with arbitrary geometry. To demonstrate this capability, we fabricate various kinds of wavy waveguides with the same diameter of ∼250 μm using the above-mentioned process. Figures 4(a) and 4(b), shows digital-camera-captured pictures of two sinusoidal hollow fibers. The amplitude and period of the waveguide in Fig. 4(a) are 125 μm and 10 mm, respectively, whereas for the waveguide in Fig. 4(b), its amplitude and period are 125 μm and 50 mm, respectively. The total length of the two waveguides is 50 mm. We also try to characterize the optical properties of these wavy waveguides by coupling the same He-Ne laser beam into them. Interestingly, for the wavy waveguide shown in Fig. 4(a), no output beam can be observed, which should be attributed to a high bending loss. However, for the wavy waveguide in Fig. 4(b), the near-field and far-field beam profiles are shown in Figs. 4(c) and (d), respectively. Unlike the straight hollow waveguide in Fig. 1, the wavy waveguide cannot support single-mode propagation in the horizontal direction (i.e., the oscillation direction of the sinusoidal function), due to the multiple reflection of the laser beam during its propagation. The multiple reflections could cause multimode formation as well as the beating between the different modes, giving rise to the two bright spots in the far field.

Table 1 Comparison of RMS roughness (R_q), average roughness (R_a), and maximum roughness (R_{max}) for samples before and after post-annealing. The size of examined area is 10 × 10 μm^2

Sample (size: 10 × 10 μm^2)	RMS (R_q) (nm)	R_a (nm)	R_{max} (nm)
Before post-annealing	120.2	101.5	616.2
After post-annealing	5.2	4.6	56.1

Table 2 Comparison of RMS roughness (R_q), average roughness (R_a), and maximum roughness (R_{max}) for samples before and after post-annealing. The size of examined area is 50 × 50 μm^2

Sample (size: 50 × 50 μm^2)	RMS (R_q) (nm)	R_a (nm)	R_{max} (nm)
Before post-annealing	360.3	277.5	2562
After post-annealing	52.4	44.0	337.5

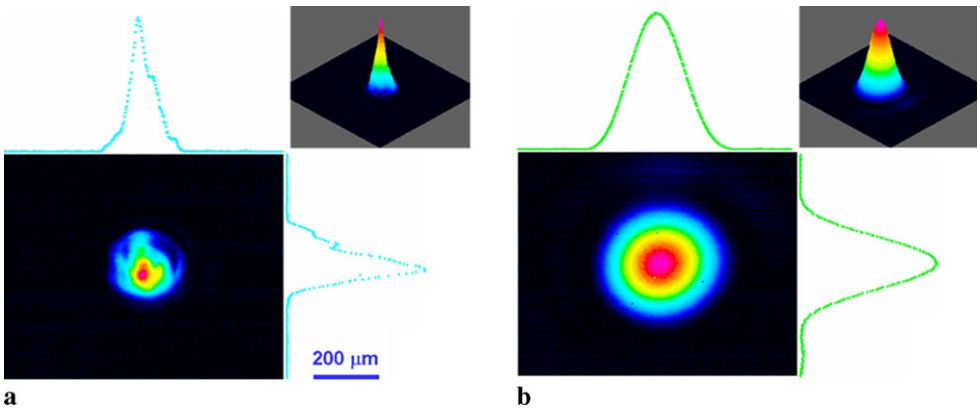

Fig. 3 (Color online) (**a**) Near-field and (**b**) far-field profiles of the He–Ne laser beam exiting from the hollow waveguide

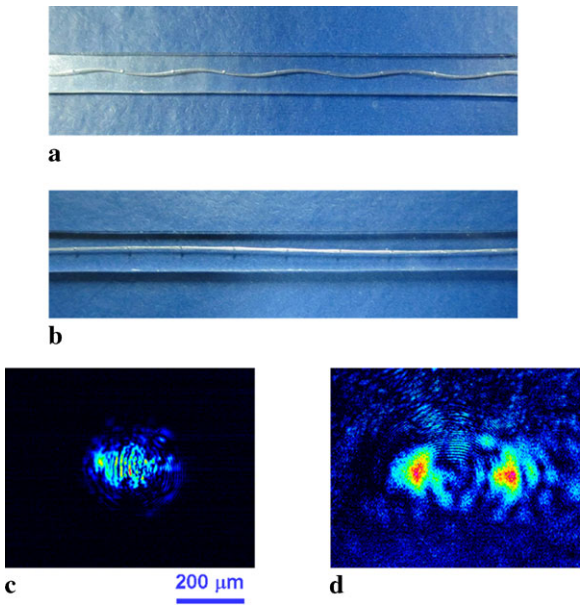

Fig. 4 (Color online) Overview images of two wavy hollow waveguides corresponding to an amplitude of 125 μm and periods of (**a**) 10 mm and (**b**) 50 mm. (**c**) Near-field and (**d**) far-field modes of the He–Ne laser beam exiting from the wavy waveguide in (**b**)

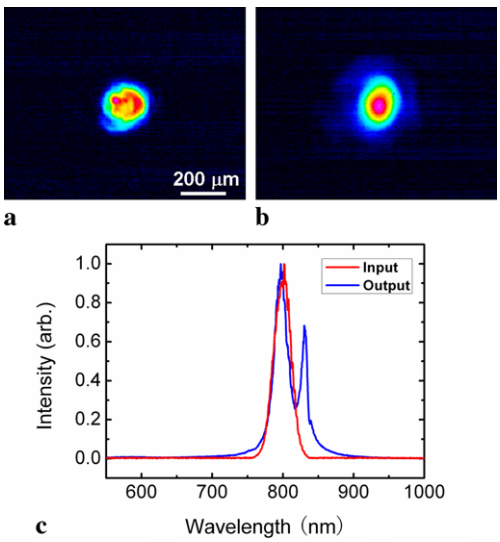

Fig. 5 (Color online) (**a**) Near-field and (**b**) far-field mode profiles of output pulses from the hollow waveguide with low input pulse energy of 586 μJ. (**c**) Comparison of spectra of input (*red curve*) and output (*blue curve*) femtosecond laser pulses

4 Spectral broadening of femtosecond pulses in the hollow waveguide

As a first attempt of using the hollow waveguide fabricated by femtosecond laser for high-field laser application, we perform the spectral broadening experiment with ∼30 fs laser pulses at 800-nm wavelength and 1-kHz repetition rate (Elite Duo, Coherent, Inc., USA). It is noteworthy that

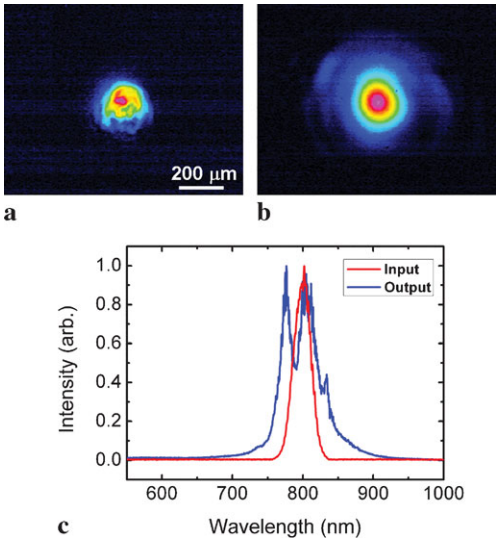

Fig. 6 (Color online) (**a**) Near-field and (**b**) far-field mode profiles of output pulses from the hollow waveguide with high input pulse energy of 906 μJ. (**c**) Comparison of spectra of input (*red curve*) and output (*blue curve*) femtosecond laser pulses

the best application for such hollow waveguide fabricated by femtosecond laser microfabrication should not be spectral broadening or pulse compression, as in these applications longer waveguides (e.g., tens of centimeters or a few meters long) are often used [2, 3]. However, as we already mentioned in the Introduction, the hollow waveguides may find important applications in the fields such as high-order harmonic generation or laser particle acceleration. Nevertheless, for evaluating the performance of the hollow waveguides fabricated by femtosecond laser for high-field laser physics application, spectral broadening experiment carried out in air is the easiest. The laser pulses are focused into the 62-mm-long hollow waveguide using a lens with a focal length of 500 mm. The beam size of output pulses from the femtosecond laser is measured to be ∼8 mm, and then the pulses pass through an aperture with a diameter of ∼4 mm. The clipped beam then reaches the front surface of the lens. First, with low-pulse energy of only ∼2 μJ, the propagation of the beam in the hollow waveguide is almost a linear optical process, and no spectral broadening can be observed (data not shown). In this case, the transmission is measured to be ∼84%. Then, we increase the pulse energy gradually in order to obtain both broad spectrum and good beam profile. When the input pulse energy is increased to 586 μJ, we measure both the near-field and far-field mode profiles as shown in Figs. 5(a) and 5(b), respectively. Clearly, both mode profiles show single-mode characteristics. In addition, we observe that the spectrum is slightly broadened toward the red side, as compared to the original spectrum of the output pulses at the ∼800 nm wavelength. A further increase of the input pulse energy to 906 μJ results in significant spectral broadening, from the

initial bandwidth of 27.2 nm (full width at half-maximum, FWHM) to 55.7 nm (FWHM), as shown in Fig. 6(c). Notably, in this case both the near-field (Fig. 6(a)) and far-field (Fig. 6(b)) images of the emanating pulses show nearly single-mode profiles. The measured transmission efficiency reaches ∼47.2% (corresponding to output pulse energy of 428 μJ). In our experiment, high-intensity femtosecond laser pulses with pulse energy up to ∼1.8 mJ are injected into the hollow waveguide and no damage is found. The successful demonstration of the spectral broadening with the hollow optical waveguide indicates that the structure is robust and can sustain high-peak intensity that is necessary for high-field laser physics experiments.

5 Conclusions

To conclude, we have successfully fabricated hollow optical waveguide in fused silica by femtosecond laser micromachining. The inner surface roughness is greatly improved by a post-annealing process for optical applications. Owing to the high surface smoothness, the total transmission of the hollow waveguide reaches ∼90%, which is close to the theoretical limit of such waveguide based on partial reflection on the inner wall (e.g., for the 6.2-cm-long hollow waveguide with a diameter of 250 μm, the calculated transmission is ∼95% [20], including both the coupling and propagation losses). We also achieve the spectral broadening of femtosecond laser pulses with the hollow waveguide, e.g., from the original spectral bandwidth of 27.2 to 55.7 nm.

The unique flexibility offered by the laser direct writing allows us to precisely tailor the geometry of the hollow waveguide, as evidenced by the wavy waveguide. In addition, it is also possible to control the other parameters of the waveguides in a spatial-selective manner, namely, each portion of the waveguide can be individually tailored by tuning the laser parameters during the laser direct writing. For example, it will be straightforward for us to fabricate a hollow waveguide composed of sections with alternative diameters by depositing different doses of laser irradiation for adjacent sections. Last but not the least, we would like to point out that with our technique, several hollow waveguides could be simultaneously fabricated and fused together to form complex photonics networks, such as beam-splitters and couplers, etc. These possibilities make our technique attractive for high-field laser physics research [21–23].

Acknowledgements The work is supported by National Basic Research Program of China (Grant No. 2011CB808102) and National Natural Science Foundation of China (Grant Nos. 10974213 and 60825406).

References

1. B. Schenkel, J. Biegert, U. Keller, C. Vozzi, M. Nisoli, G. Sansone, S. Stagira, S. De Silvestri, O. Svelto, Opt. Lett. **28**, 1987 (2003)
2. M. Nisoli, S.D. Silvestri, O. Svelto, Appl. Phys. Lett. **68**, 2793 (1996)
3. A. Suda, M. Hatayama, K. Nagasaka, K. Midorikawa, Appl. Phys. Lett. **86**, 111116 (2005)
4. A. Paul, R.A. Bartels, R. Tobey, H. Green, S. Weiman, I.P. Christov, M.M. Murnane, H.C. Kapteyn, S. Backus, Nature **421**, 51 (2003)
5. M. Zepf, B. Dromey, M. Landreman, P. Foster, S.M. Hooker, Phys. Rev. Lett. **99**, 143901 (2007)
6. E. Esarey, C.B. Schroeder, W.P. Leemans, Rev. Mod. Phys. **81**, 1229 (2009)
7. W.P. Leemans, B. Nagler, A.J. Gonsalves, Cs. Tóth, K. Nakamura, C.G.R. Geddes, E. Esarey, C.B. Schroeder, S.M. Hooker, Nat. Phys. **2**, 696 (2006)
8. K. Nakajima, private discussion
9. A. Marcinkevičius, S. Juodkazis, M. Watanabe, M. Miwa, S. Matsuo, H. Misawa, J. Nishii, Opt. Lett. **26**, 277 (2001)
10. M. Masuda, K. Sugioka, Y. Cheng, N. Aoki, M. Kawachi, K. Shihoyama, K. Toyoda, H. Helvajian, K. Midorikawa, Appl. Phys. A **76**, 857 (2003)
11. K. Sugioka, M. Masuda, T. Hongo, Y. Cheng, K. Shihoyama, K. Midorikawa, Appl. Phys. A **79**, 815 (2004)
12. Y. Cheng, K. Sugioka, K. Midorikawa, M. Masuda, K. Toyoda, M. Kawachi, K. Shihoyama, Opt. Lett. **28**, 1144 (2003)
13. Y. Cheng, K. Sugioka, K. Midorikawa, Opt. Lett. **29**, 2007 (2004)
14. F. He, Y. Cheng, Z. Xu, Y. Liao, J. Xu, H. Sun, C. Wang, Z. Zhou, K. Sugioka, K. Midorikawa, Y. Xu, X. Chen, Opt. Lett. **35**, 282 (2010)
15. F. He, Y. Cheng, L. Qiao, C. Wang, Z. Xu, K. Sugioka, K. Midorikawa, J. Wu, Appl. Phys. Lett. **96**, 041108 (2010)
16. F. He, H. Xu, Y. Cheng, J. Ni, H. Xiong, Z. Xu, K. Sugioka, K. Midorikawa, Opt. Lett. **35**, 1106 (2010)
17. S. Kiyama, S. Matsuo, S. Hashimoto, Y. Morihira, J. Phys. Chem. C **113**, 11560 (2009)
18. Y. Cheng, K. Sugioka, K. Midorikawa, M. Masuda, K. Toyoda, M. Kawachi, K. Shihoyama, Opt. Lett. **28**, 55 (2003)
19. V. Maselli, R. Osellame, G. Cerullo, R. Ramponi, P. Laporta, L. Magagnin, P.L. Cavallotti, Appl. Phys. Lett. **88**, 191107 (2006)
20. S.D. Silvestri, M. Nisoli, G. Sansone, S. Stagira, O. Svelto, in F. Kärtner (ed.) *Few-Cycle Laser Pulse Generation and its Applications* (Springer, Berlin, 2004), pp. 265–291
21. H. Xiong, R. Li, Z. Zeng, Y. Zheng, Y. Peng, X. Yang, X. Chen, H. Zeng, Z. Xu, Phys. Rev. A **75**, 051802(R) (2007)
22. J. Liu, R. Li, Z. Xu, Phys. Rev. A **74**, 043801 (2006)
23. F. Krausz, M. Ivanov, Rev. Mod. Phys. **81**, 163 (2009)